Uncertainty Quantification of Electrospray Thruster Array Lifetime

IEPC-2019-317

Presented at the 36th International Electric Propulsion Conference
University of Vienna, Austria
September 15-20, 2019

Benjamin A. Jorns*, Alex Gorodetsky†, Ian Lasky‡, Angela Kimber§, and Peter Dahl ¶
Department of Aerospace Engineering, University of Michigan, Ann Arbor, MI 48109, USA

Benjamin St. Peter‖ and Rainer Dressler**
Spectral Sciences, Inc., Burlington, MA 01803, USA

A numerical investigation into the performance and lifetime of an electrospray array thruster of pressurized-capillary emitters is presented. A series of modules based on the Electrospray Propulsion Engineering Toolkit (ESPET) are employed to create a reduced fidelity model for the operation of a colloidal thruster. New modules are added to this toolkit to enable predictions of lifetime including scaling laws for beam divergence, propellant deposition on the extractor grid, and failure due to backstreaming current. The impact of uncertainty on performance and lifetime is also quantified. Sources of uncertainty considered include both physics-based model parameters and manufacturing tolerances A Monte Carlo analysis is applied to generate probability distribution functions for key performance parameters including thrust, efficiency, and specific impulse. The median performance values are shown to agree qualitatively with typical performance conditions for this pressure-fed configuration of an electrospray array. Probability of failure curves are also generated for both a single emitter and an array of emitters operated on the same power supply. It is found that as the uncertainty in design parameters or the number of emitters increases, the lifetime of the array decreases. Parametric analyses are also performed with the goal to optimize thruster performance while accounting for uncertainty. To this end, it is shown that there is an optimum throttling point for achieving maximum predicted total impulse. This proof of concept thus illustrates the potential capability of this approach for guiding design and optimization.

*Assistant Professor, bjorns@umich.edu
†Assistant Professor
‡Graduate student
§Graduate student
¶Graduate student
‖Senior Scientist
**Chief Scientist

Nomenclature

P_R	= Reservoir pressure
Q	= Volumetric flow rate
R_c	= Inner radius of capillary
L_c	= Length of capillary
T_{prop}	= Propellant temperature at emission point
R_e	= Radius of extractor aperture
V_b	= Bias voltage from extractor to emission tip
I_b	= Beam current
θ_d	= Divergence angle of plume
d	= Distance from extractor to capillary
ϕ_J	= Jet potential
ϕ_c	= Polar angle of capillary with respect to the normal of extractor plane
θ_c	= Azimuthal of capillary
θ_E	= Angle subtended by extractor
δR	= Offset of capillary from centerline
Q_E	= Volumetric propellant flow to extractor
ϵ_0	= Permittivity of free space
ϵ	= Relative permittivity of propellant
γ	= Surface tension of propellant
K	= Conductivity of propellant
ρ	= Mass density of propellant
V_o	= Onset voltage for spraying
l_o	= Divergence model lengthscale fit parameter
μ	= Propellant viscosity
R_{drop}	= Radius of droplet formed on extractor from deposition
h_{drop}	= Height above extractor of droplet formed from deposition
V_{drop}	= Volume of droplet formed from deposition
t^*	= Time to failure
I_s	= Specific impulse
T	= Thrust
η	= Efficiency

I. Introduction

Electrospray thrusters offer a potentially game-changing capability for in-space electric propulsion.[1] These devices employ a strong electric field to extract charged droplets directly from microscopic electrohydrodynamic structures, "Taylor cones," formed in conducting liquids. In principle, they can yield high specific impulse (> 1000 s) at higher efficiency (> 80%) and thrust density compared to state of the art electric propulsion devices. The high theoretical efficiency is a benefit of the fact that there is no energy penalty for ionizing the propellant in these systems since it is already doped with charged carriers. The higher thrust density stems from the microscopic scale of the thrust-producing area of these systems.

While individual electrospray emitters have attractive performance metrics, their low thrust has proven to be a major limitation in the widespread adoption of this technology for in-space propulsion. Indeed, typical thrust levels for a single emitter are on the micro-Newton scale. This force is only useful for a limited number of missions.[2] To increase the thrust level to magnitudes that could be used for state of the art electrospray mission architectures (e.g. station-keeping and orbit raising), it is necessary to use multiple emitters. Thrust is increased by manufacturing arrays of closely-packed emitters in a single thruster head, all firing concurrently. If it is possible to create these arrays with emitters that are sufficiently closely spaced while maintaining the nominal efficiency of each emitter, in principle electrospray arrays could offer an order of magnitude improvement in thrust density over state of the art technology at a higher efficiency. Indeed, it has been suggested that if electrospray arrays could be achieved with thousands or even hundreds of thousands of emitters firing simultaneously, this technology would supplant most electric propulsion systems.[1]

A number of technical challenges have precluded the development of flight-ready large scale (>1000 emitters) arrays to date. These include concerns about performance, integration, and lifetime. For example, to maintain a high thrust density, it is necessary to build arrays with emitters as closely packed as possible. However, it is not clear if and how emission sites will interact with one another as the distance between them decreases. The performance of the device, as represented by thrust, specific impulse, and efficiency, may suffer.[3] With respect to integration, the modeling of electrospray array plumes is still a nascent field with open questions related to key processes such as plume neutralization and spacecraft/plume interactions. Finally, the problem of lifetime is particularly pressing and unresolved for large-scale emitters. Individual emitters can fail for a number of reasons.[4] For example, arcing and electrical shorts can result when propellant builds up on the extractor and the acceleration electrodes that establish the electric field in the thruster.[5] In a multiplexed system, depending on the electrical configuration of a circuit, the failure of even one emitter can short the entire array electrically.[6] The major obstacle for lifetime is thus being able to build systems with hundreds or thousands of emitters that can fire simultaneously for thousands of hours (a typical electric propulsion mission duration) without incurring the failure of even one emitter. To be sure, there are on-going efforts to explore different array combinations. Building small-scale arrays with fewer than 28 emitters has proved to be a tractable problem with thruster lifetimes exceeding several thousand hours.[5,7] On the other hand, lifetime for large, multiplexed arrays continues to remain limited to a few hundred hours.[6]

The uncertainties that result from manufacturing tolerance may be one of the most critical obstacles that has precluded scaling arrays to larger size. Indeed, while it is possible to construct and verify individual emitters to meet lifetime and performance requirements, manufacturing challenges related to tolerance, alignment, and repeatability can prohibit the ability to replicate these performance metrics on a larger scale. For example, as the number of emitters is increase, a few outliners may emerge with substantially reduced life, thus posing a risk to the whole thruster. With this in mind, the problem of uncertainty points to a pressing need for tools to help quantify and understand the risk of its effect as arrays are scaled in size. The goal of this work is to address this need by employing a probabilistic approach in which we leverage of a combination of Monte Carlo sampling and reduced fidelity models of emitter operation.

This paper is organized in the following way. In the first section, we describe the emitter architecture we investigate for this work and the numerical engineering tool we employ, the Electrospray Propulsion Engineering Toolkit (ESPET) created by Spectral Sciences, Inc. We also classify uncertainties in the model based on its origin and discuss our methods for propagating this uncertainty into lifetime assessment. In the following section, we present results from our analysis oriented toward addressing the questions outlined above. Finally, in the last section, we discuss our results in the context of limitations of the current model and how the model may be extended to other emitter architectures.

II. Model Description

We discuss in the following section the chosen emitter architecture, details of the numerical model, and the methods for uncertainty quantification we employ.

A. Emitter configuration

We consider in this work one of the simplest forms of electrospray emitters, the pressure-fed capillary tube operating strictly in droplet mode (i.e. not in the pure ionic regime). We explore this architecture for this proof of concept as it is one of the most widely-studied and characterized methods for generating electrosprays.[8] The modeling of this system similarly lends itself to simplified scaling laws easily understood and implemented in our engineering toolkit. We show in Fig. 1 a schematic for a single emitter where we have denoted key elements of the geometry. The pressure, P_R, in the reservoir of ionic liquid drives the propellant at a volumetric flow rate Q through a hollow capillary tube with length L_c and internal radius R_c. The propellant is forced through the end of the capillary, forming a meniscus at the end with temperature T_{prop}. A potential bias, V_B, is applied to this meniscus via a high-voltage discharge supply connected directly to the conducting liquid and a flat extractor electrode located a distance, d, downstream of the capillary tip with an aperture radius, R_E. These two dimensions form the emitter angle ϕ_E. The applied potential deforms the meniscus into the canonical "Taylor cone" singularity that emits a jet of charged droplets with total beam current I_b. These droplets are accelerated in the jet by strong electric fields to high speed. This acceleration results in a beam of droplets with characteristic divergence angle, θ_d, that propagates downstream and through the extractor aperture. It is the acceleration of these particles that gives rise to the thrust of an individual emitter.

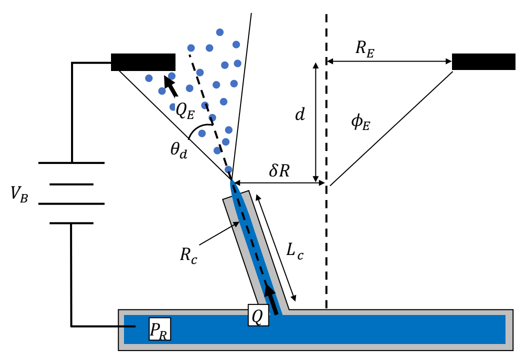

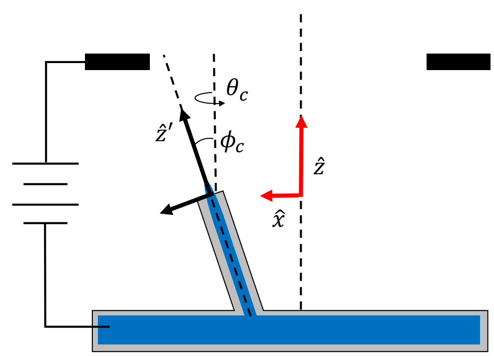

Figure 1: Schematics of the pressure-fed capillary electrospray showing side views with (a) labeled dimensions and (b) coordinate and angle definitions. The prime coordinates are aligned with the capillary while the unprimed are aligned with the center of the extractor. The capillary displacement from centerline is specified to be in the $\hat{x}$ direction.

In this work, we also consider three non-idealities in capillary operation. First, while ideally the resulting kinetic energy of the droplets would scale with the applied voltage, V_b, from the extractor to liquid, in practice local losses due to processes such as Ohmic heating reduce the effective potential drop of the ions. We denote this loss in potential in the jet as ϕ_J. Second, the alignment of the capillary tube and the downstream extractor will not be perfect. There will be variations in the polar angle, ϕ_c, defined with respect to the normal vector to the extractor plane and the azimuthal angle, θ_c. There also will be variations in capillary offset from concentricity with the extractor, δR. Finally, because of these misalignments and the inherent divergence of the angle, some of the beam propellant can deposit and collect on the downstream extractor at a rate, Q_E. As we discuss in the following, this deposition ultimately may result in arcing back to the emitter from the extractor, shorting out the circuit.

To further narrow the focus of this study, we confine our analysis to the propellant EMI-BF4 that is passed through a silica capillary tube and extracted by a thin aluminum plate. We similarly restrict our investigation to flow rates ranging from Q = 0.1 - 5 nl/s and extractor distances ranging from d =1.0 to 1.4 mm with an aperture radius of R_E = 0.8 to 1.2 mm. We elect to consider this emitter configuration and range of values for two reasons. First, they ensure that the emitter remains in droplet mode. And second, these values are consistent with the experimental, data-driven studies[11] we have performed to date to develop scaling laws for beam divergence. By confining our analysis to a similar parameter space over which this study was performed, we improve the confidence in our use of these scaling laws. We also make the strong assumption here that when arrayed, individual emitters do not interact with one another. Their failures and performance are thus independent of one another.

B. Modules for electrospray operation

We use modules adapted from the Electrospray Propulsion Engineering Toolkit (ESPET) created by Spectral Sciences, Inc. to model the operation of the capillary geometry discussed in the preceding section. ESPET leverages physics-based as well as semi-empirical scaling laws drawn from the electrospray community to build subroutines that allow a user to model multiple propellants and geometries and to predict key performance metrics such as thrust, efficiency, and current. The tool has been evaluated against a number of experimental datasets and shown to yield both qualitative and quantitative agreement for a number of different emitter configurations.[12] As a result, ESPET is well-suited tool for guiding the design of large scale emitter arrays. With that said, despite its wide range of existing capabilities, ESPET to date does not contain modules to evaluate thruster lifetime or failure modes. We thus present in the following not only a summary of the current ESPET modules we used for this investigation, but we also introduce two new modules for plume divergence and failure due to propellant accumulation on the extractor.

1. Beam current

As discussed in Sec. A, we confine our investigation to high flow rates where we know emission can be maintained and the emission current is dominated by droplet emission. We therefore neglect the role of field evaporation of ions and the possibility of entering the mixed ion-droplet or pure ionic regime. Subject to these constraints, the beam current is given by the simplified semi-empirical expression:[13]

$$I_b = \sqrt{\frac{\epsilon_0 \gamma^2}{\rho}} \left[6.2 \sqrt{\frac{Q \rho K}{\gamma \epsilon_0 \sqrt{\epsilon - 1}}} - 2 \right], \tag{1}$$

where ϵ_0 is the permittivity of free space, ρ denotes the propellant mass density, γ is the surface tension, K is the conductivity, and ϵ is the relative permittivity of the propellant. Physically, this expression shows that the current emitted by a Taylor cone is dictated by the rate at which fluid can be provided to the tip, Q.

2. Onset voltage

The onset voltage, V_o is the minimum voltage bias, V_b, as applied between the extractor and emitting surface necessary to lead to the emission of droplets. This is based on the analytical derivation from Martinez-Sanchez[14] for the deformation of a meniscus in the presence of an applied electric field assuming a hyperboloidal interface:

$$V_o = \tanh^{-1}(\eta_0) \left(1 - \eta_0^2\right) \sqrt{\frac{a^2 \gamma}{\epsilon_0 R_c}}, \tag{2}$$

where we have defined $a = 2d/\eta_0$ with

$$\eta_0 = \left(1 + \frac{R_c}{d}\right)^{-1/2}. \tag{3}$$

This result shows functionally that as the radius of the emitter increases or the distance from tip to emitter increases, the voltage required for onset also increases. Physically, this is a consequence of the fact that the increase in both length scales reduces the effective electric field at the emitter tip. In our following study, we select a bias voltage $V_b > V_o$ such that we ensure the spray is always active.

3. *Flow rate*

As this is a pressurized capillary, we assume that the flow rate is driven entirely by the pressure at the reservoir and the hydraulic impedance of the feed line and capillary. Given the scale and low rate of the liquids, we employ the Poiseuille approximation:

$$Q = P_R \frac{\pi r_c^4}{8\mu L_c}, \tag{4}$$

where μ denotes the viscosity of the propellant. This expression shows intuitively that the increase in pressure differential will promote more flow. Similarly, there is a strong dependence on the geometry of the capillary.

4. *Divergence angle*

The ESPET tool currently accepts the plume divergence angle as a user-supplied input value, instead of calculating it from other parameters.[12] In a recent work,[11] we have derived a semi-empirical expression for this value:

$$\theta_d = \tan^{-1}\left[R_0(P)\left(\frac{l_0}{d}\right)\frac{I_b}{V_b}\right]^{3/4}, \tag{5}$$

where l_0 denotes a best fit parameter with average value $l_0 = 3.1 \pm 0.5$ mm and we have introduced an effective resistance that depends on the propellant properties:

$$R_0(P) = \left(\frac{9}{2}\right)^{4/3}\left(\frac{1}{2\pi\sqrt{2}\epsilon_0 f(\epsilon)}\sqrt{\frac{\rho\epsilon}{\gamma K}}\right)^{2/3}, \tag{6}$$

where $f(\epsilon)$ is an empirical function introduced by de la Mora[15] and has a value of $f(\epsilon) \approx 8$ for EMI-BF4. The physical principle underlying this derivation is that the divergence of the beam is driven by space charge effects as the beam propagates from the emitter to the downstream extractor. As the current increases, the number of charge carriers in the region increases, driving a larger repulsing field between ions. As the voltage increases, the velocity of ions is sufficiently high emerging from the jet that the expansion is curtailed. The dependence on extractor-to-emitter tip distance reflects the weak acceleration that can result from the external electric field that exists in the emitter to extractor gap.

There are a number of assumptions that underpin the derivation of Eq. 5. The first is we assume the droplet beam is mono-dispersive with a constant mass to charge ratio for the droplets. This is consistent with all of the modules for pure droplet emission within ESPET. The second assumption we make is that the current density of the beam is a top-hat distribution that spreads out through a conical solid angle subtended by the divergence angle, θ_d:

$$I_\Omega \propto H(\theta_d - \theta) \tag{7}$$

where I_Ω is the current per unit solid angle (Asr^{-1}), θ is the polar angle measured with respect to the axis of emission of the spray, and we have introduced the Heaviside step function:

$$H(x) = \begin{cases} 1 & x \geq 0 \\ 0 & x < 0. \end{cases} \tag{8}$$

This latter assumption about the angular current distribution is not strong, as plume based studies have shown the current distribution for an emitter array can deviate from a top-hat, approaching Gaussian or super-Gaussian.[10,16] For our work, however, we note that in previous experimental studies that have examined divergence angle for pressure-fed capillaries operating in droplet mode,[16] the current distributions were found to be approximately top-hat. In the absence of direct plume data for our modeled geometry and propellant, we proceed then with the assumption that the top-hat current distribution is a valid approximation.

As a last comment, it should be noted here we only calibrated Eq. 5 for one propellant, EMI-BF4, operating in the droplet emission mode with one capillary geometry. The universality of this expression has yet to be established. We thus confine our investigation to an emitter type that shares the mean design properties (radius, capillary length, and extractor geometry) with the emitter used in this previous study. This provides increased confidence for the use of this simplified expression in our analysis.

5. Deposition on extractor

The mass deposition on the emitter is a key parameter that impacts the lifetime and performance of the device. It can result from high plume divergence or misalignment between the capillary and the extractor aperture. In order to account for these effects (shown graphically in Fig. 1), we write

$$Q_E = Q\left[1 - \frac{1}{2\pi\left(1-\cos\theta_d\right)}\int_{-\infty}^{\infty}\int_{-\infty}^{\infty}\left(H\left[R_e - \sqrt{(x-\delta R)^2+y^2}\right]\right.\right. \tag{9}$$

$$\left.\left. H\left[\theta_d - \tan^{-1}\left(\left|\frac{\sqrt{(x')^2+(y')^2}}{z'}\right|\right)\right]\frac{\vec{r'}\cdot\hat{z}}{(r')^{3/2}}\right)_{z\to d} dxdy\right], \tag{10}$$

where $H()$ denotes the Heaviside step function and we have defined $\vec{r'} = x'\hat{x}' + y\hat{y}' + z\hat{z}'$. The prime coordinates are in the frame of reference of the capillary emitter with its $\hat{z}'$ axis aligned with the emitter tip (Fig. 1b). The unprimed coordinates are in the frame of reference of the extractor where $\hat{z}$ is defined along the normal to the plane of the extractor with the extractor in in the $\hat{x}$ direction. We have assumed without loss of generality that the displacement of the capillary from concentricity.

We can relate the two coordinate systems through the following transformations:

$$\hat{x}' = \overline{\overline{R}}_z(\phi_c)\cdot\overline{\overline{R}}_x(\theta_c)\cdot\hat{x} \tag{11}$$

$$\hat{y}' = \overline{\overline{R}}_z(\phi_c)\cdot\overline{\overline{R}}_x(\theta_c)\cdot\hat{y} \tag{12}$$

$$\hat{z}' = \overline{\overline{R}}_z(\phi_c)\cdot\overline{\overline{R}}_x(\theta_c)\cdot\hat{y} \tag{13}$$

$$(x', y', z') = \left[\overline{\overline{R}}_z(\phi_c)\cdot\overline{\overline{R}}_x(\theta_c)\right]^T\cdot(x, y, z), \tag{14}$$

where we have denoted the rotation matrices, $\overline{\overline{R}}_z(\phi_c)$ and $\overline{\overline{R}}_x(\theta_c)$ and T denotes transpose.

Physically, Eq. 10 is predicated on the assumption that the spray with respect to the capillary axis will follow a top-hat distribution subtending a polar angle θ_d with respect to this capillary axis. In order to determine how much of this spray will impact the extractor, we transform from the coordinate system of the spray plume to the coordinate system of the extractor. This requires two rotation matrices, one for the polar angle deflection of the capillary from vertical, θ_c and one for any twisting this capillary may have, ϕ_c. Finally, in order to model the displacement of the capillary and the extractor, we displace the circle represented by the extractor by δ_r with respect to the origin defined by the capillary's location.

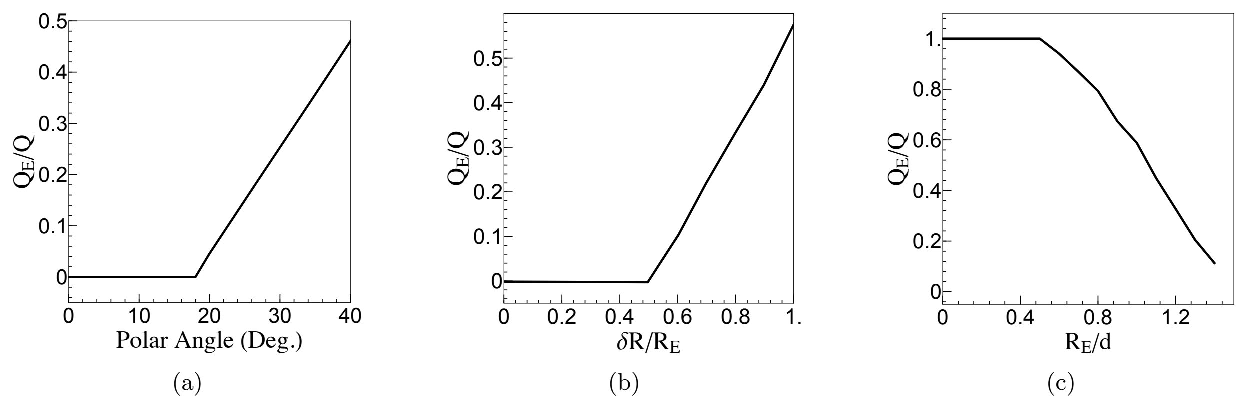

Figure 2: Fraction of total mass flow intercepted by extractor for (a) varying polar angle of the capillary tip with $\delta R = 0, R_E = d$, (b) varying displacement of tip with $R_E = d$ and $\phi_c = 0°$ and (c) varying extractor aperture radius with $\delta R = 0$ and $\phi_c = 0°$. The divergence angle is $\theta_d = 30°$ and the azimuthal rotational angle $\theta_c = 0°$ for all cases.

We illustrate qualitatively the trends represented by Eq. 10 in Fig. 2 where we show three plots of the fraction of intercepted current as the polar angle is varied, as the displacement is varied, and as the aperture size as widened. As can be seen from these results, as the deflection of the capillary and its alignment with the extractor worsen, the fraction of intercepted current increases. However, as the aperture radius increases, for fixed plume divergence angle, more current can pass through the geometry.

6. Failure from arcing

The dominant failure mode we consider for this pressurized system is arcing that can occur from propellant that has accumulated on he capillary-facing side of the downstream extractor. While it is understood that this arcing results when a critical amount of propellant has been deposited, it is still an open question as to how to quantify this critical volume. For example, in the Busek-built nine-emitter thruster produced for the Lisa Pathfinder mission, the extractor grids are porous and therefore can absorb liquid.[9] This has led to a proposed onset criteria that breakdown will occur when these porous grids have been saturated. On the other hand, for non-porous extractors such as those more commonly used for large scale arrays,[6] the criteria for breakdown due to propellant accumulation is still poorly understood, and to our knowledge, not been modeled in detail to date. For this proof-of-concept of an engineering tool, we propose a physically-intuitive though ultimately unvalidated process.

To this end, we qualitatively describe the process for breakdown in Fig. 3. First, we assume that any propellant that is deposited on the extractor will pool into a single droplet. The shape of this droplet in turn will be driven by the volume of mass deposited, the surface tension, and the contact angle of the propellant on the extractor. As the amount of deposited propellant increases, the size of the droplet will increase, leading to a wider base, R_{drop} and an increased height off the extractor, h_{drop}. At some critical point, the onset requirement for breakdown (Eq. 2) will be satisfied (allowing $R_c \rightarrow R_{droplet}$ and $d \rightarrow d - h_{droplet}$ thereby leading to a Taylor cone and backspraying to the capillary. At this point, it is assumed that this spraying facilitates the formation of low-resistance path from extractor to capillary tip, resulting in shorting and failure.

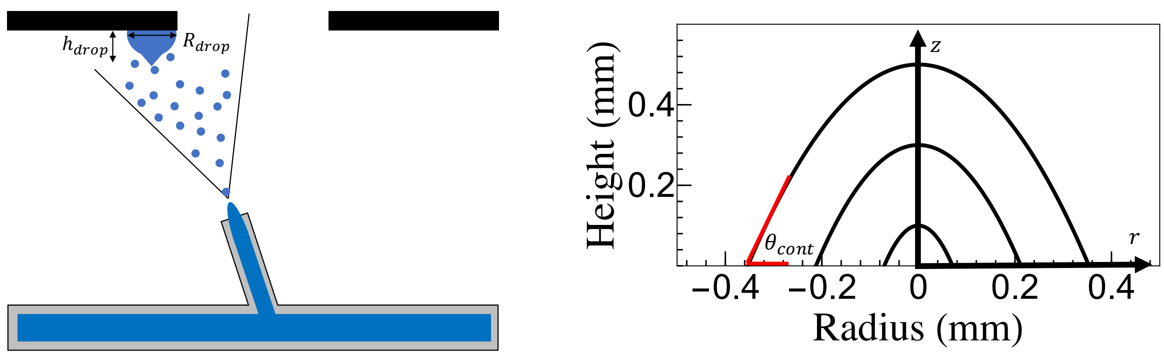

Figure 3: (a) Schematic of failure mode due to backspraying from downstream droplet. b) Numerical solutions for droplet shape on aluminum or three different volumes of EMI-BF4.

To model this process, we need expressions for the droplet shape, radius, and height as functions of total deposited volume. To this end, we numerically solve the Young-Laplace equation for a droplet:

$$\gamma \left(\frac{z''(r)}{(1 + (z'[r])^2)^{3/2}} + \frac{z'(r)}{r(1 + (z'[r])^2)^{1/2}} \right) = \Delta P, \tag{15}$$

where γ denotes the surface tension and ΔP is the internal pressure of the droplet, z is the height of the droplet from the substrate, and r is the horizontal displacement from droplet centerline (Fig. 3b). Physically, the left hand side represents the force from surface tension at the droplet/vacuum interface which is balanced against internal pressure in the droplet. We note here that we assume that the formed droplets will be smaller than the characteristic capillary length, ($R_{drop} < l_{cap} = 1.7$ mm) for the modeled propellant, EMI-BF4. We therefore neglect hydrostatic pressure in this formulation.

To simplify our analysis, we assume that droplets that deposit on the extractor will equilibrate to room temperature, yielding an EMI-BF4 with surface tension of $\gamma = 0.04$ N/m. We similarly assume, consistent with the work of Dandavino,[17] that the surface contact angle of the propellant on aluminum is $\theta_{cont} = 70.5°$. Armed with these values, we solve Eq. 15 iteratively. We select a height, $z(0) = h_{drop}$ of the droplet from

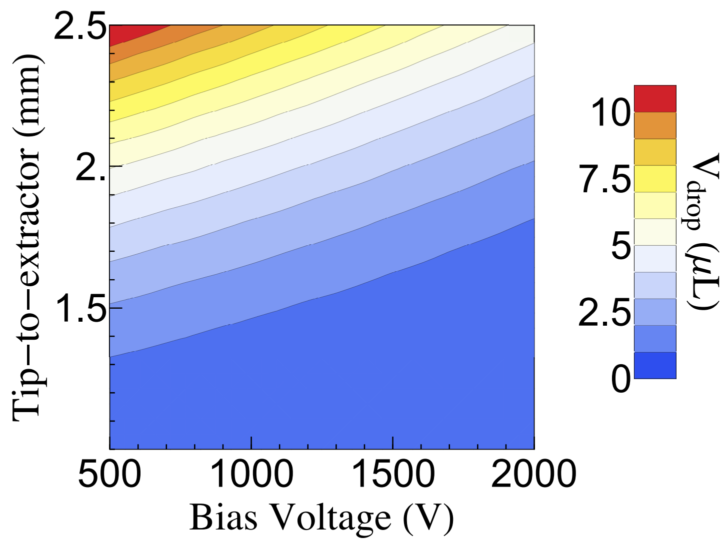

Figure 4: Parametric plot of critical volume of deposited propellant to result in break down as a function of bias voltage and extractor to capillary tip.

the extractor and set the initial slope of the droplet at this height to be $z'(0) = 0$. We then guess at a value of ΔP and integrate the equation until $z(R_{drop}) = 0$. We compare the slope of the solution at this angle, $\theta_{cont} = \tan^{-1}[z'(R_{drop})]$ to the known contact angle of 70.5° and iterate on the internal pressure, ΔP until we achieve the correct angle. We repeat this process for a range of droplet heights. The results are shown graphically in Fig. 3b.

To relate these results to the onset voltage, we integrate numerically over the volume of the droplet, V_{drop} and substitute the values of R_{drop} and h_{drop} into Eq. 2. We show in Fig. 4 a parametric plot of the volume of the droplet for onset voltage to occur as a function of extractor to tip distance and bias voltage. As can be seen, as the initial distance between the extractor and capillary decreases or the bias voltage increases, the required volume of a droplet to lead to breakdown lowers. In practice during simulation runs, we use the known values of V_b and d to estimate the volume, $V^*_{drop}(d, V_b)$ that will result in backspraying. We then can relate this volume to time to failure, t^* with the mass deposition formulation (Eq. 10):

$$t^* = \frac{V^*_{drop}}{Q_e}. \tag{16}$$

7. Propellant

As can be seen from the above simplified models, the propellant properties factor heavily into predictions for electrospray operation. Key properties include the conductivity, K, the surface tension, γ, the relative permittivity, ϵ, and the viscosity, μ. All of these attributes are influenced by external factors including exposure to atmosphere, water absorption, and temperature. For the purpose of this study, we assume the propellant has been controlled to eliminate the influence of the former two effects and instead consider only the role of propellant temperature, e.g. $K(T_p), \gamma(T_p), \epsilon(T_p), \mu(T_p)$. To estimate these dependencies, we leverage the embedded database in ESPET for EMI-BF4 which tabulates values drawn from previous work for these properties. We note here that interestingly, the temperature of the propellant at the emission tip is not well-known or modeled as local effects such as Ohmic heating can drastically influence this parameter. We thus treat it as an unknown model parameter in our assessments.

8. Performance

Finally, we outline here the simple models for performance implemented in ESPET. Consistent with the previous modules, we assume that the beam current follows a top-hat distribution and that the beam is monodispersive. With this in mind, we can write

$$T = (Q - Q_e)\,\rho\sqrt{2\,(V_b - \phi_J)}\sqrt{\frac{I_b}{\rho Q}}\cos(\theta_d)\,; \qquad I_{sp} = \frac{1}{g}\frac{T}{\rho Q}; \qquad \eta = \frac{1}{2}\frac{T^2}{\rho Q V_b I_b}, \tag{17}$$

where T denotes thrust, I_{sp} is specific impulse, and η is the thruster efficiency. Here in the thrust equation, we explicitly have accounted for the adverse impact of mass flow lost to the extractor Q_E, the loss in potential acceleration from ϕ_J, and the beam divergence ϕ_d.

C. Uncertainty Quantification

We use Monte Carlo to perform a probabilistic assessment of the emitter output with respect to uncertainties in the system Table 1 summarizes the components of the models and parameters that are subject to uncertainty. These uncertainties are grouped into two classes: physics-based model parameters and manufacturing tolerances. The physics-based inputs correspond to our lack of certainty in the modules outlined in the previous section. They represent aspects of the spray that we do not know how to model or uncertainty in the fit coefficients of semi-empirical models (c.f. Eq. 5). For the architecture we have outlined in the preceding discussion, the three physics-based uncertainties include the temperature of the propellant, T_p, the jet potential drop, ϕ_J, and the lengthscale in the divergence model, l_0. The manufacturing uncertainties are known quantities that stem from machining tolerance and alignment. For this study, these consist of the radius of the aperture in the extractor, the tip-to-extractor distance, the orientation of the tip with respect to the extractor, and the capillary dimensions. Finally, we note here that we treat two parameters as precisely known (i.e., negligible uncertainties), the bias voltage, V_b, and the reservoir pressure, P_B. These both can be controlled and measured with a high degree of precision for an actively-pressurized system.

Table 1: Classification of uncertainties for code inputs

Parameter	Description	Source of Uncertainty
T_p	Propellant temperature at emitter tip	Physics-based model parameters
ϕ_J	Jet potential	Physics-based model parameters
l_0	Divergence model fit parameter	Physics-based model parameters
R_c	Capillary inner radius	Manufacturing tolerance
l_c	Capillary length	Manufacturing tolerance
R_e	Radius of aperture in extractor	Manufacturing tolerance
δR	Capillary offset from concentricity	Manufacturing tolerance
θ_c	Angle of capillary with respect to vertical	Manufacturing tolerance
ϕ_c	Azimuthal angle of capillary	Manufacturing tolerance
P_B	Reservoir pressure	No uncertainty
V_b	Bias voltage	No uncertainty

III. Results

A. Performance assessment for baseline case

Our performance assessment targets quantifying the confidence in two metrics: performance and lifetime. For the performance assessment, since we assume that all emitters in an array are non-interacting and therefore statistically independent, we can perform a one-step, Monte Carlo uncertainty propagation for a single-emitter. We specify upper and lower bounds for the parameters (Table 1), both manufacturing and physics-based, and assume these parameters are uniformly distributed. We then sample from these distributions of parameters 10^6 times, run ESPET for each sampled set of inputs, and generate probability distribution functions (PDF) for each parameter.

For our baseline case in this study, we used the range of input parameters shown in Table 2. We chose the median of the dimensions of the capillary to be consistent with the single emitter experimental setup that guided the calibration of the model for the divergence model in Eq. 5.[11] The bounds on these ranges are typical or estimated uncertainties in manufacturing and alignment. For example, we assume that an operator will be able to maintain concentricity of the emitter tip with the center of the extractor, δR, to within 0.1 mm and with an angular accuracy of $\phi_c = 20°$. We selected the operating conditions, bias voltage and pressure, such that when we ran the simulation with the median values of the geometry shown in Table 2 we found values consistent with those measured in Ref. 11, i.e. flow rates $Q \sim 0.5$ nl/s and currents $I_b \sim 1.0$ uA . Finally, we also verified that when we used the median values from the ranges specified in Table 2 that there was no grid interception ($Q_E = 0$). This median case thus in principle would have an infinite lifetime, and indeed, this is how most arrays initially would be designed. Our initial study of this baseline case thus is the equivalent of examining the role of non-ideal alignment as well as uncertainty in our understanding of the models in impacting our confidence in the model predictions.

Table 2: Input ranges for ESPET Monte Carlo run

Parameter	Baseline	Reduced uncertainty
T_p	$[300, 350]$ K	$[300, 350]$ K
ϕ_J	$[0, 200]$ V	$[0, 200]$ V
l_0	$[2.6, 3.6]$ mm	$[2.6, 3.6]$ mm
R_c	$[7, 9]$ μm	$[7.5, 8.5]$ μm
l_c	$[4.8, 5.2]$ cm	$[4.9, 5.1]$ cm
d	$[1.0, 1.4]$ mm	$[1.1, 1.3]$ mm
R_E	$[0.8, 1.2]$ mm	$[0.9, 1.1]$ mm
ΔR	$[0, 0.1]$ mm	$[0, 0.05]$ mm
θ_c	$[0, 20]$ deg.	$[0, 5]$ deg.
ϕ_c	$[0, 360]$ deg.	$[0, 360]$ deg
P_B	2×10^5 Pa	2×10^5 Pa
V_b	2000 V	2000 V

With this in mind, we show in Fig. 5 PDFs for key outputs from the model. In interpreting these results, the peak in each PDF represents the most probable value of the output while the confidence in this prediction scales inversely with the spread of each PDF. We note that the most probable predicted breakdown voltage is consistent with the values we reported in Ref. 11 for a similarly-configured capillary emitter. The fact that our input voltage, V_b is higher than all of the values of the PDFs suggests that all cases we consider would in fact be spraying. The most probable values for performance, e.g. a specific impulse of $I_{sp} = 210s$, divergence angle of $\theta_d = 32°$ and thrust $T = 1.0\mu N$ are all consistent with pressure fed capillaries that have been reported to date.[18] Indeed, the low specific impulse is a direct function of the low charge to mass ratio of capillaries operating in droplet emission mode. The predicted efficiency, $\sim 70\%$ is high, though likely a substantial over prediction. This stems from the fact that the predicted efficiency functionally only depends on the divergence angle and the intercepted current. The effects of polydispersivity are negligible due to the negligible ionic current. We finally note that the most probable divergence angle is smaller than the most probable value of the extractor aperture angle, ϕ_E. This suggests that in the most probable case, the beam in this configuration will pass through the aperture with minimal interception. This is consistent with our initial choice of median values to ensure that there is a minimum overlap. Allowing for the spread in each of these divergence angles, however, there can be cases where the plume divergence will exceed the angle of the extractor aperture, giving rise to impingement on the extractor. Moreover, since we have considered the effects of finite misalignment of the grids in both angle and displacement, we anticipate that there will be cases where there can be some extractor interception. This is supported by the plot of the average fractional value of deposition shown in Fig. 5. This result physically suggests that because of the impact of uncertainty in manufacturing (as well as the underlying physical processes), a given emitter has a finite chance of leading to extractor impingement and ultimate failure. We quantify this risk in the following section.

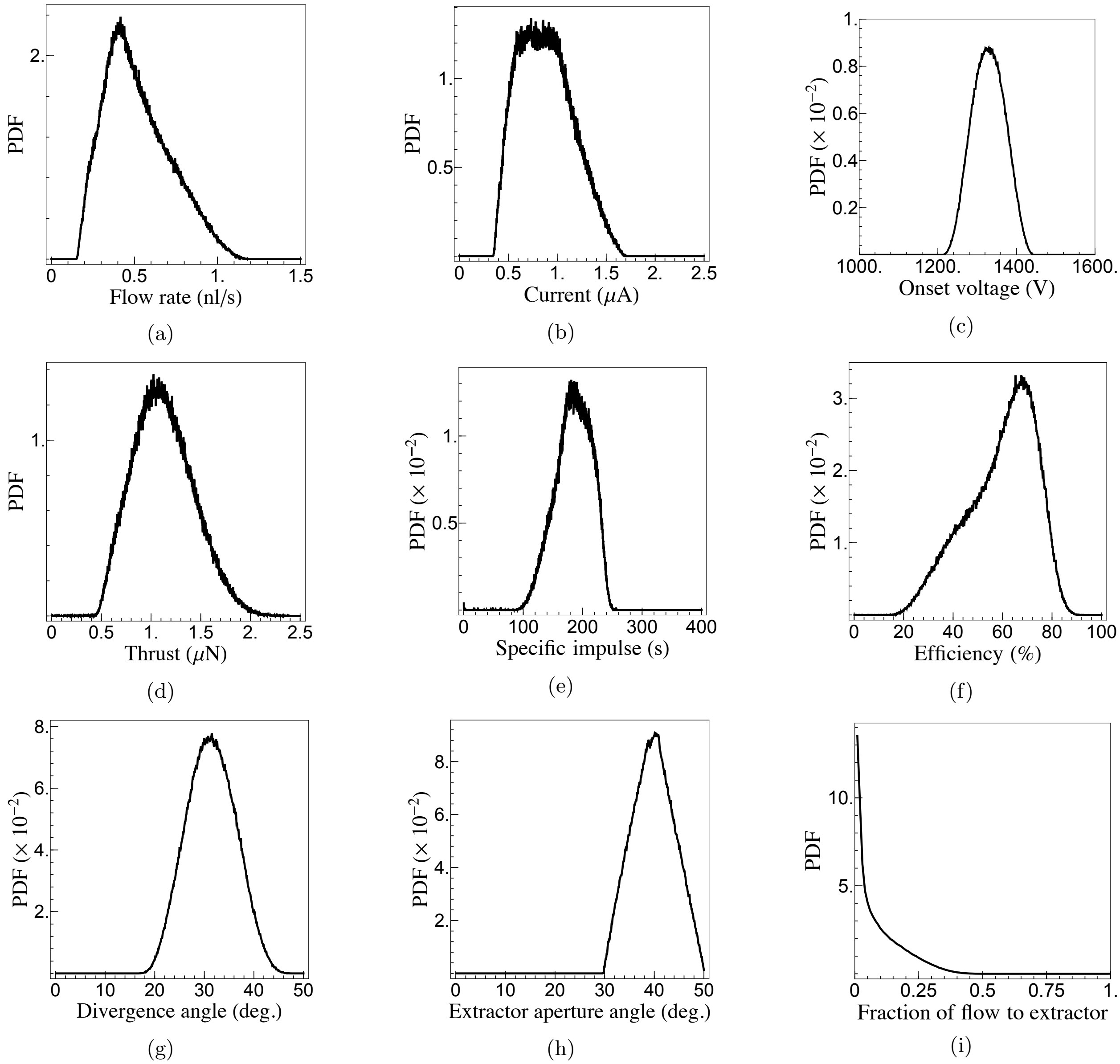

Figure 5: Performance outputs from ESPET for a single emitter after Monte Carlo run with input parameters dictated by Table 2.

B. Lifetime assessment for baseline case

Generating lifetime predictions is more nuanced than the performance assessments as we need to treat the classes of uncertainty different. Our aim is to provide conditional lifetime assessments given fixed models. To this end, we first sample randomly from the distributions of the three physics-based parameters (Table 1). We fix these values and then sample 1000 points randomly from the design parameters subject to manufacturing uncertainty. We run the model for these 1000 cases and create a a series of bins in time, Δt, each 15 minutes long. At each bin (corresponding to total run time of $t_j = j * \Delta t$), we evaluate the number of results from the simulation that have reached failure, i.e. $t^* < t_j$ (Eq. 16) and record the total fraction that has failed, $p(t_j)$. In this way, we assign to each bin the probability of failure for an individual emitter at this point in time. Once we have binned this set of data, generating a curve $p(t_j)$, we iterate by again sampling once from the physics-based uncertainties and running the model for 1000 samples from the manufacturing uncertainties. We repeat this process 1,000 times to generate a family of curves that represent the failure of probability.

We show in Fig. 6 the median from these curves (solid) as well as the first and third quartiles (dashed). The overall shape of the failure curve stems from the uncertainty in the manufacturing tolerance. It reflects uncertainty in how the system was built. The variance in the failure curve (as represented by the quartiles) reflects uncertainty in our simplified models for how the system works. If we had perfect knowledge of the physics, the quartiles would collapse. Physically, we can interpret this result in the following way by considering the simplifying case that we know the physics perfectly, e.g., considering median curve to correspond to this case. If we were to build a set number of single emitters according to the manufacturing tolerances specified in Table 2 and run each individually over time, we would see that the fraction of emitters that failed would follow the curve shown in Fig. 6. If all the emitters were built precisely to the median value in the ranges shown in Table 2, none of them would fail. However, because of manufacturing tolerance and misalignment, some of the emitters will have a finite of amount of current deposited on the extractor (Fig. 5i). These emitters will fail over time. Even those emitters that have finite impingement, however, deposit at sufficiently slow rates that all of them will survive for a minimum of $\sim$ 1 hour. After this time, some of the emitters from the lot will fail. Eventually, after 15 hours, all emitters that had any amount of current impingement on the extractor will have failed. The remaining $\sim$ 50% have dimensions such that all of the emitted current passes through the aperture without impingement, thereby in principle having unlimited lifetime. This is why the curve does not asymptote to 1 instead of the plotted value of 0.5. Another interpretation is that every time an emitter is built to tolerance, there is a 50% chance it will never fail. With that said, because there is uncertainty in the underlying physical models, there is corresponding uncertainty in the probability of failure curve. This is captured by the quartile ranges shown in Fig. 6.

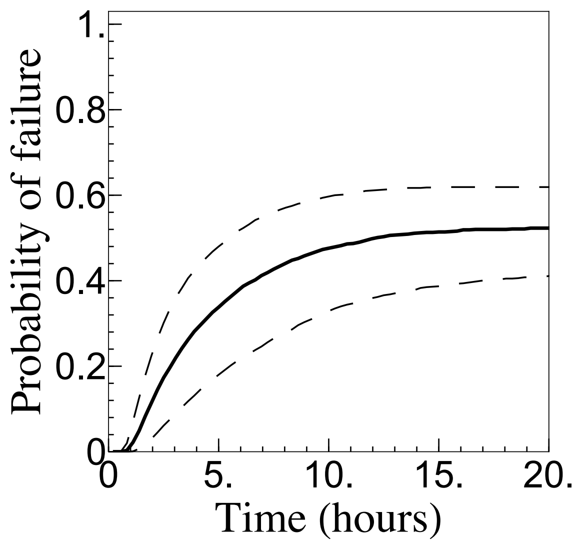

Figure 6: Probability of failure for a single emitter subject to the uncertainties outlined in Table 2. The solid black represent the median while the dashed lines are the first and third quartiles

The preceding discussion pertains to a single emitter, though in practice, we are interested in quantifying the properties for arrays. As we have assumed that the emitters are statistically independent, key performance metrics such as efficiency and specific impulse will remain unchanged. The thrust, current, and flow rate will scale with the number of emitters, N_{em}. To estimate the failure rate, we make the strong assumption that when we build an array of emitters, if even one emitter fails, it will cause the entire thruster to fail. This is a reasonable assumption provided the emitters and extractors are all on a shared electrical circuit. With this in mind, we can translate the probability of failure for a single emitter $p(t_j)$ to the failure rate of an array:

$$P(t_j) = 1 - (1 - p(t_j))^{N_{em}} . \tag{18}$$

We evaluate Eq. 18 in Fig. 7a-c for arrays with 10, 100, and 1000 emitters using the probability for a single emitter failure from Fig. 6. As this result shows, the probability of failure now approaches unity and the lifetime of the array decreases to an hour as the number of emitters increases in the array. As a caveat, we note here that these failure times are two orders of magnitude lower than state of the art 100-emitter systems.[6]

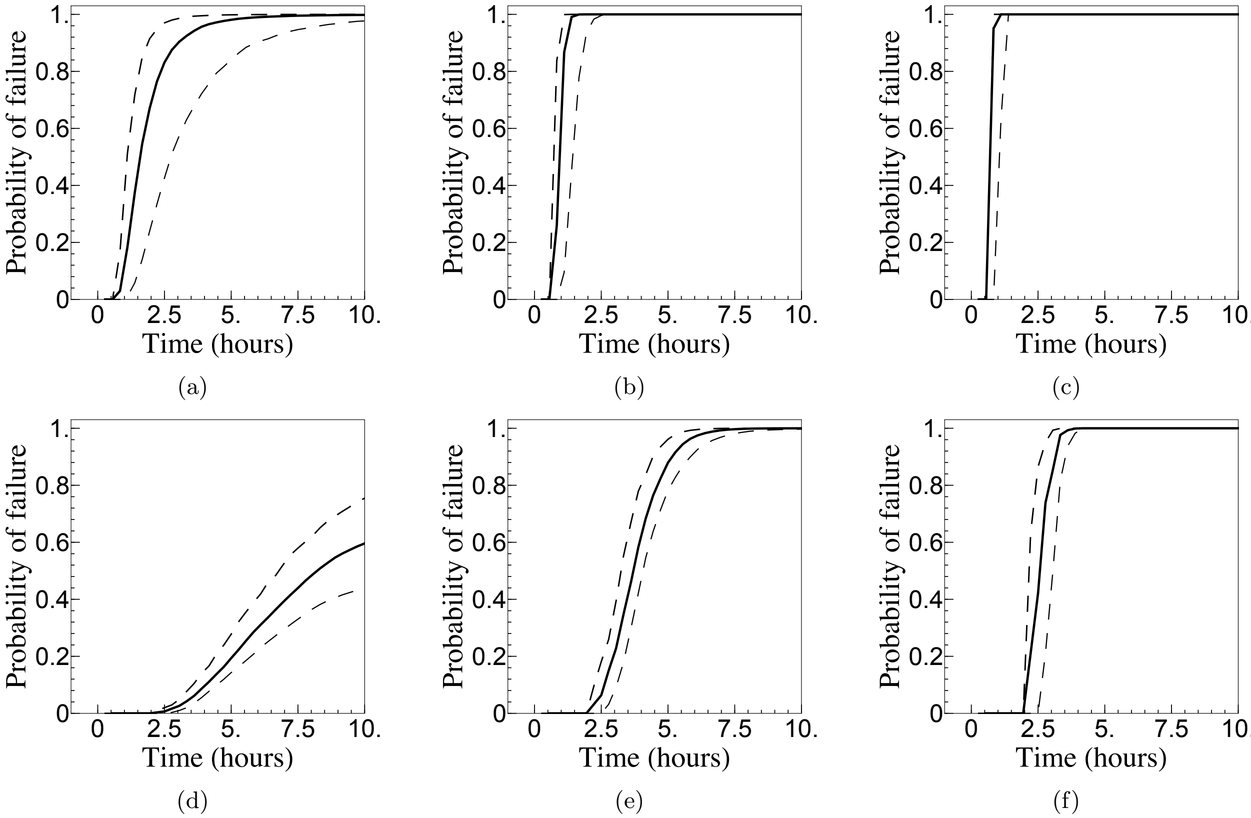

Figure 7: Probability of failure for (a) a 10 emitter array, (b) a 100 emitter array, and (c), a 1000 emitter array for the baseline parameters shown in Table 2. Probability of failure for (d) a 10 emitter array, (e) a 100 emitter array, and (f), a 1000 emitter array for the reduced uncertainty case shown in Table 2. The solid black represent the second quartile while the dashed lines are the first and third quartiles.

The decrease in lifetime with the number of emitters is an intuitive result since as the number of emitters increases, the probability of one emitter being at an extreme point of the tolerances is greater—leading to an earlier failure. More significantly, this result underscores the fact that even if an array configuration is designed such that its mean properties ensure that no current will be intercepted by the extractor grid, the physical limitations of manufacturing tolerance and repeatability will result in thrusters that will still fail.

C. Lifetime assessment with improved manufacturing tolerance

In practice, for arrays with a smaller number of emitters, lifetime can be improved by manufacturing a large lot and checking each emitter individually. As shown in Fig. 6, there are some emitter configurations in the tolerance band where this is no failure. These correspond to the cases where there is no overlap between the beam and the extractor. If a user only needs a single emitter, they can produce a lot of emitters and select the ones with the favorable alignment. This approach, of course, is not practical or plausible as the number of emitters is increased. As an alternative, if we could reduce the tolerance such that more emitters were created at the median case where there is no overlap between spray and extractor (i.e. make the curves narrower in Fig 5 g-h), we also would be able to increase life.

D. Lifetime assessment by changing thruster operating condition

To demonstrate this quantitatively, we have repeated the Monte Carlo analysis for a second set of improved higher precision tolerances (Table 2) and show the results for a 10,100, and 1000 emitter array in Fig. 7(d-f). It is evident here that the average lifetime does improve with improved manufacturing tolerance, increasing the value to 2 hours. This result demonstrates that at the outset of design, these types of parametric analyses can establish minimum requirements for manufacturing tolerances to achieve a given lifetime. The additional insight afforded by our approach is that we recognize even an array with no tolerance uncertainty still will have a chance of failure due to uncertainty in the underlying physical models. The approach described here in principle can guide the choice of tolerance to ensure that within a designated confidence interval, a given array will survive.

Recognizing that we only have a limited capacity to reduce the manufacturing tolerance, we note that we may be able to improve thruster lifetime for a fixed geometry by changing the operating condition. We focus here on one well-known aspect of performance, the thrust level. Indeed, one of the major advantages in electing an actively pressurized system is that the current and therefore thrust can be adjusted by changing the applied pressure. With this in mind, we have performed a parametric assessment of the thrust and lifetime as a function of reservoir pressure for the baseline case (Table 2) assuming a 100 emitter array. Fig. **??** shows the median values of thrust with error bars corresponding to the first and third quartiles of the PDF while the lifetime plots correspond to the time at which there is 50% probability failure with error bars corresponding to the confidence intervals.

It can immediately be seen from this plot that thrust increases with reservoir pressure. This is to be expected for this system as the flow rate correlates with pressure. Interestingly, however, the thrust level appears to plateau with increasing pressure. This counterintuitive result is a consequence of the fact that the divergence of the beam scales directly with beam current (which in turn scales with flow rate). With increasing pressure, more current is thus intercepted by the extractor array and the beam divergence widens, thus limiting how much directed thrust is generated. The increase in intercepted rate to the extractor combined with the overall high flow rate yield a lower overall lifetime. This is reflected by the nonlinear decrease exhibited in Fig. 8 with reservoir pressure where we see a two order of magnitude drop from lifetime at the lowest pressure (1000 Pa) to lifetime at the highest values (500 kPa).

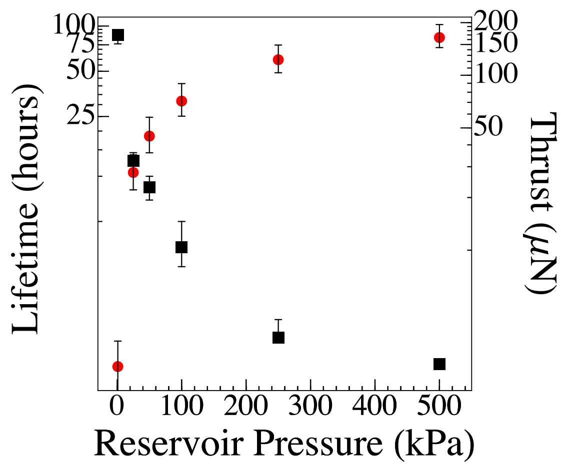

Figure 8: Predicted thrust (red) and lifetime (black) at 50% failure probability as a function of reservoir pressure for a 100 emitter array. Simulation performed for the baseline case in Table 2.

An interesting implication of the dependence shown in Fig. 8 is that the thruster lifetime can be improved by electing to use a lower flow rate. However, this conclusion can be misleading when considered in the context of the thruster performance. From an applied perspective, a more relevant parameter is to evaluate total impulse, $I_T = Tt^*$ imparted by the system before failure. This is the key metric for understanding how much momentum the propulsion system can impart to the spacecraft over its lifetime. Fig. 9a shows the total impulse as a function of thrust for a 100 emitter array. It is immediately evident that this curve exhibits an optimum (outside uncertainty). In other words, this result would suggest that there is an optimal thrust level for maximizing the total impulse that can be imparted by the 100 emitter propulsion system. As an extension of this, we recall (Fig. 7) that as the number of emitters increases, the lifetime of the array decreases. On the other hand, the thrust level increases with the number of emitters. This suggests there may be a trade between emitter numbers and total impulse. To illustrate this notionally, we show in Fig. 9b the total impulse for a single emitter as a function of thrust level. The error bars are much larger on this plot, which follows the fact that the failure curves have more uncertainty. However, following the median values, this result would suggest that a single emitter, operating at a fraction of the thrust level can actually

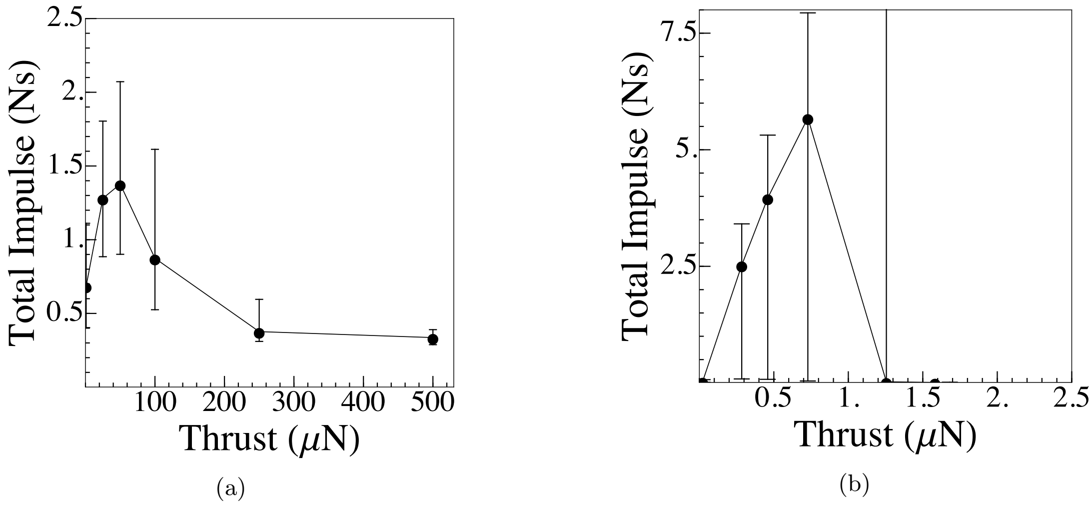

Figure 9: Predicted total impulse as a function of thrust level for (a) a 10 emitter array and (b) a single emitter.

deliver a higher total impulse than the array. Naturally, the single emitter will need to run longer, but if thrust level is not a driver, this may drive the designer to a single array configuration. This unexpected result illustrates a novel and enabling featuring of a probability-based engineering model.

IV. Discussion

The results in the previous sections have served to illustrate the utility of combining reduced fidelity models with rigorous uncertainty quantification. In particular, we have examined how this combination can yield predictions for performance and lifetime and may also be useful for guiding the key design requirements such as manufacturing tolerance. We also have shown how these tools may even be used to identify optimal thruster configurations. These are the features that can be leveraged to achieve the ultimate goal of exploring design space to identify the array configurations that have the highest likelihood of achieving mission requirements (performance and lifetime).

With that said, there are a number of caveats and limitations to the analysis that we discuss here. First, we mention that the predicted lifetimes for our arrays are orders of magnitude lower than state of the art systems (c.f. Ref. 2, 6, 7). This is a consequence of our decision to baseline our analysis on a simple and unoptimized experimental setup[11] instead of an actual thruster system. The value of this work lies in the demonstration of process and capability instead of pointing to a useable flight-like system. The next extension would be to apply this tool to more realistic thruster arrays and validating the predictions against performance measurements and any known failure rates.

We note as well that there are a number of simplifying assumptions we have made to facilitate a faster model. These include assuming a top-hat current distribution, mono-dispervisity of the beam, negligible emitter interactions, negligible transients, and a failures mode that is dominated by droplet accumulation. The last assumption in particular has yet to be validated experimentally and is currently simply an ansatz informed by intuition and observation. The first four assumptions similarly are not strictly valid, even for simplified capillaries, and can introduce additional error to the predictions. The problem of cross-emitter coupling is a particularly poorly understood aspect of arrays. Indeed, by neglecting the role of cross-emitter effects, we have limited the ability of our model to evaluate key and pressing questions facing the community right now such as thruster how closely emitters can be packed. There may be simple scaling laws available to approximate these effects that may be incorporated in ESPET. But, to date, these have yet to be identified. Additional insight may come from more sophisticated models for the difference processes, e.g. current generation and transients. Though, higher fidelity typically will come at the expense of modeling time, thereby reducing the ability to perform uncertainty quantification with random sampling.

As another caveat, we have confined our analysis to arguably one of the least complex and well-studied emitter configuration, a pressurized capillary fed emitter in an array that has a single-point failure mode (one emitter failure destroys the array). This was driven in large part by the simplicity of the known scaling laws for this system as well as the fact that the divergence model we have developed in previous work was based on this configuration. In each case, the scaling was semi-empirical and calibrated against data over a range of values. For example, the divergence model was only calibrated for 0.7-1.4 mm of tip-to-extractor distance. If we confine our simulations to this parameter space, we can have a high degree of confidence in the modeling predictions. However, modeling geometries and configurations beyond this range raises the question of extensibility. It cannot rigorously be argued that without fully physics-based models that reduced fidelity models like ESPET can be used to predict entirely new geometries. There is the possibility that in geometries close to the parameter space where the models were calibrated, e.g. 1.5 mm for tip-to-extractor, may continue be accurate. However, moving further away from this regime will decrease confidence.

Functionally, this problem of extensibility can be handled in multiple ways. First, and ideally, the understanding of the underlying physical process (e.g. the mechanisms driving divergence) can improve and therefore guide a refined model. Second, absent improved physics, we can try to quantify the reduced confidence that results when the models are applied to parameter space outside where they were calibrated. This confidence should decrease as the model is extended beyond the parameter space. For example, the error bars on data-driven fit coefficients, e.g. l_0 should increased as the model is applied to regimes where this model has not been calibrated. Deciding how to rigorously do this variation in the uncertainty is an active area of research. Finally, as a more time-consuming but more straight forward data-base driven approach, we could expand the data-set where data calibration is performed, thereby extending the applicability of the model.

This last technique of increasing the data-set can lead to parameter spaces that are prohibitively large. For example, in order to be fully comprehensive for the capillary we have considered in this work, we would need to characterize how the divergence angle depends on flow rate, voltage, current, and all of the geometric factors we have defined. This leads to a parameter space with at least seven dimensions. Absent doing a full experimental characterization over this database, techniques based on optimal experimental design can be performed to help more intelligently sample the parameter space.

As a last comment related to the uncertainty quantification, we note that although the probability distributions (Fig. 5) appear to be largely normally distributed, they do have skew features, suggesting non-normal effects and potentially even the existence of tails. These features cannot easily be captured with a simple Monte Carlo scheme. This poses a particular problem for lifetime predictions of arrays. Indeed, as can be seen in Eq. 18, the failure probability of an array depends nonlinearly on the probability of failure of a single emitter. Finite but small probability of failures can drastically affect the shape of the failure curve. We may not be able to resolve these marginal cases with simple scaling. Alternative techniques such as polynomial chaos expansion should be explored to better quantify these uncertainties.

In summary, despite all of these caveats, we emphasize here that the process we have explored, i.e. combining engineering model tools with uncertainty quantification, is not to be used as a tool for generating high-fidelity predictions of lifetime for single emitters. The predictions of lifetime for highly-engineered flight systems such as the propulsion system for Lisa Pathfinder would be qualitative at best.[2] Rather, this tool is to be used as a means for narrowing down the wide parameter space of different array geometries and operating conditions that should be explored experimentally to try to achieve performance metrics, e.g. increased lifetime and/or impulse. For example, we have already demonstrated the capability to identify unexpected optimal operation. This information can be leveraged to prototype and build a new thruster design. The results from these measurements similarly can be coupled back into the modules underlying the model, helping refining the models when predictions are off, thus improving the fidelity of the code. Through this iterative process, the ultimate goal is to be able to drastically reduce the development time for electrospray thruster arrays.

V. Conclusion

We have explored the use of an engineering based numerical tool for electrospray thrusters combined with uncertainty quantification to assess the lifetime and performance of electrospray arrays based on pressure-fed capillaries operating on the ionic propellant, EMI-BF4. We have combined a series of semi-empirical scaling laws with novel models for plume divergence and electrospray failure to generate our predictions with confidence bars. We have shown how there are two distinct sources for uncertainty in the modeling of these devices: uncertainty in the semi-empirical scaling and uncertainty related to the manufacturing tolerance. We have treated each distinctly in our lifetime assessment of these devices, showing how confidence in the physical models can modify the predictions for the probability of failure of these arrays. We have explored the dependency of failure rate on several key factors showing that the lifetime will decrease as the number of emitters powered by the same source is increased and that the lifetime will improve if the manufacturing uncertainties are reduced. We also have performed a limited parametric investigation, showing that this tool can be used to identify optimal design conditions for achieving key requirements such as higher total impulse. While we have noted that there are several limitations and caveats to our findings, our results do illustrate the potential use of these types of engineering tools in guiding the design of electrospray arrays. This is a particularly critical utility given the wide parameter space of electrospray array configurations that can be explored and the challenge in prototyping and testing these systems.

Acknowledgments

This work was supported by an Early Stage Innovations grant from NASA's Space Technology Research Grants Program. The authors would also like to acknowledge the technical guidance from and discussions with Dr. John Yim of the NASA Glenn Research Center.

References

[1] Dankanich, J. and Lozano, P., "Dual Mode Green Propulsion for Revolutionary Performance Gains with Minimal Recurring Investments,," *Planetary Science Visison 2050 Workshop*, 2017.

[2] Demmons, N. R., Hruby, V. J., Courtney, D., Ziemer, J. K., and Marrese-Reading, C., *Ground and On-Orbit Thruster Performance Comparison for the Lisa Pathfinder Colloid MicroNewton Thrusters*, American Institute of Aeronautics and Astronautics, 2019/08/31 2018.

[3] Deng, W. and Gomez, A., "Influence of space charge on the scale-upof multiplexed electrosprays," *Aerosol Science*, Vol. 38, 2007, pp. 1062–1078.

[4] Brikner, N., *On the Identification and Mitigation of Life-limiting Mechanisms of Ionic Liquid Ion Sources Envisaged for Propulsion of Microspacecraft*, Ph.D. thesis, MIT, 2015.

[5] et al, J. Z., "Colloid Microthruster Flight Performance Results from Space Technology 7 Disturbance Reduction System," *35th International Electric Propulsion Conference, Georgia Institute of Technology*, 2017.

[6] D. Krejci, F. Mier-Hicks, C. F. P. L. A. H. S. and Martel, F., "Design and Characterization of a Scalable ion Electrospray Propulsion System," *34th International Electric Propuls, IEPC-2015-149.*, 2015.

[7] Jelem, D. e. a., "Performance Mapping and Qualification of the IFM Nano Thruster FM for in Orbit Demonstration," *35th International Electric Propulsion Conference, Georgia Institute of Technology, IEPC-2017-24*, 2017.

[8] Gañán-Calvo, A. M., López-Herrera, J. M., Herrada, M. A., Ramos, A., and Montanero, J. M., "Review on the physics of electrospray: From electrokinetics to the operating conditions of single and coaxial Taylor cone-jets, and AC electrospray," *Journal of Aerosol Science*, Vol. 125, 2018, pp. 32 – 56, From Electro-Hydro-Dynamics of liquids for the production of charged droplets by Electro-Spray to applications for tailored Materials (aerosols, powders, coatings) and Environment.

[9] Thuppul, A., Wright, P., and Wirz, R. E., *Lifetime Considerations and Estimation for Electrospray Thrusters*, American Institute of Aeronautics and Astronautics, 2019/08/31 2018.

[10] Wirz, R. E. e. a., "Electrospray Thruster Performance and Lifetime Investigation for the LISA Mission," *AIAA Propulsion and Energy 2019 Forum*, American Institute of Aeronautics and Astronautics, 2019/08/31 2019.

[11] Dahl, P. N., Kimber, A. M., and Jorns, B., *Data-Driven Scaling Laws for Electrospray Plume Divergence from a Capillary Tube*.

[12] St. Peter, B., Dressler, R. A., Chiu, Y.-h., Fedkiw, T., Wang, Y., and Song, H., "Electrospray Propulsion Engineering Toolkit (ESPET)," *35th International Electric Propulsion Conference Georgia Institute of Technology*, 2017, pp. IEPC–2017–206.

[13] Gañán-Calvo, A., Dávila, J., and Barrero, A., "Current and droplet size in the electrospraying of liquids. Scaling laws," *Journal of Aerosol Science*, Vol. 28, No. 2, 1997, pp. 249 – 275.

[14] Martinez-Sanchez, M., "16.522 Space Propulsion. Massachusetts Institute of Tech- nology OpenCourseWare." .

[15] De La Mora, J. F. and Loscertales, I. G., "The current emitted by highly conducting Taylor cones," Vol. 260, 1994, pp. 155–184.

[16] Gamero-Castano, M., "The Structure of Electrospray Beams in Vacuum," *Journal of Fluid Mechanics*, Vol. 604, 2008, pp. 339–368.

[17] S. Dandavino, C. Ataman, H. S. C. R. and Stark, J., "Microfabrication of Capillary Electrospray Emitters and ToF Characterization of the Emitted Beam," *32ndInternational Electric Propulsion Conference, Wiesbaden, Germany, IEPC-2011-131*, 2011.

[18] Gamero-Casta, M. and Hruby, V., "Electrospray as a Source of Nanoparticles for Efficient Colloid Thrusters," *Journal of Propulsion and Power*, Vol. 17, No. 5, 2001, pp. 977–987.